Nasir, S.; Ali, M.; Ramirez Hoyos, P.; Froehlich, K.; Cervera, J.; Mafe, S.; Ensinger, W. (2021). Ionic conduction through single-pore and multipore polymer membranes in aprotic organic electrolytes. Journal of Membrane Science. 635:1-10. https://doi.org/10.1016/j.memsci.2021.119505

Ionic conduction through single-pore and multipore polymer membranes in aprotic organic electrolytes

Saima Nasir[a,b], Mubarak Ali[a,b,*], Patricio Ramirez[c], Kristina Froehlich[a], Javier Cervera[d], Salvador Mafe[d], and Wolfgang Ensinger[a,e]

[a]*Department of Material- and Geo-Sciences, Materials Analysis, Technische Universität Darmstadt, Alarich-Weiss-Str. 02, D-64287 Darmstadt, Germany*

[b]*Materials Research Department, GSI Helmholtzzentrum für Schwerionenforschung, Planckstr. 1, D-64291, Darmstadt, Germany*

[c]*Departament de Física Aplicada. Univ. Politècnica de València. E-46022 Valencia, Spain*

[d]*Departament de Física de la Terra i Termodinàmica, Universitat de València, E-46100 Burjassot, Spain*

[e]*Centre for Synthetic Biology, Technische Universität Darmstadt, 64283 Darmstadt, Germany*

*Corresponding authors:

Email address: m.ali@gsi.de

ABSTRACT

We experimentally characterize the ionic conduction of single and multipore nanoporous membranes in aprotic organic electrolytes. To this end, soft-etched (SE) membranes with pore diameters in the nanometer range and track-etched (TE) membranes with pore diameters in the tens of nanometers range are investigated. In aqueous conditions, the membrane ionic conduction rates follow the same trend of the bulk solution conductivities. However, the ionic transport through the narrow SE-nanopores dramatically decreases in aprotic electrolytes due to the formation of solvated metal cations and their adsorption on the pore surface. The current-voltage recordings of single conical nanopores in aprotic electrolyte solutions with different water mole fractions reveal that the solvated metal ion (M) species $[M–(solvent)_4]^+$ formed in acetonitrile solvent are more tightly bounded to the pore walls compared with the cationic chelates obtained in propylene carbonate solvent. The basic findings reported here should be of interest for ionic/molecular nanofiltration processes in non-aqueous conditions as well as for moisture sensitive and energy storage nanofluidic devices.

Keywords: nanoporous membranes; ionic conductance; aprotic organic solvents; nanofluidic devices; ion current rectification

1. Introduction

Membrane ionic selectivity and conduction are regulated by the interfacial zone at the liquid/solid interface in confined geometries. The pore charges generated by ionized functional groups or surface dipoles generate an interfacial polar region, the electrical double layer [1-5], which controls transport properties such as ionic selectivity and conduction [6-8]. Biological ion channels based e.g. on α-hemolysin embedded in lipid bilayers have become a model system to study ion transport at the nanoscale [9-11] but the fragility of the lipid layer limits practical applications. On the contrary, biomimetic synthetic membranes based on solid-state materials, e.g., ceramics and polymer foils exhibit both chemical and mechanical robustness in different working conditions [12-15]. Moreover, the pore dimensions (shape and size) and chemical characteristics can be tuned on demand for every application [16-26], usually under aqueous conditions. Transport through nanoporous membranes have also been investigated in the cases of ionic liquids [27] and organic electrolytes [28-30]. For instance, Yin *et al.* have reported current rectification inversion in glass nanopipettes due to the adsorption of tetraphenylarsonium cations on the pipette surface under organic electrolyte conditions [30]. Also, Siwy and coworkers have described these ionic current rectification phenomena with detail in track-etched single-cylindrical and conical nanopores for the cases of polycarbonate and polyethylene terephthalate membranes in aprotic organic solvents [28, 29]. The electrokinetic and ion transport through nanoporous membranes have also been investigated in nonaqueous and organic solvent/water mixture based electrolytes[31-33].

Non-aqueous and organic solvents are used in the chemical and pharmaceutical industries for the synthesis, separation, and purification of organic molecules [34-37]. Moreover, energy storage devices such as capacitors and batteries also require anhydrous conditions [38-42]. Therefore, basic research on the aqueous sensitivity of ionic conduction in nanoporous membranes under organic solvent conditions is much needed.

We experimentally study here single-pore and multipore membranes immersed in electrolyte solutions prepared in water and aprotic solvents as well as their mixtures. The aprotic solvents are anhydrous propylene carbonate (PC), acetonitrile (ACN) and dimethylformamide (DMF). The multipore polyimide (PI) membranes with subnanometer pore are fabricated by the selective dissolution of latent ion tracks with an organic solvent through soft-etch (SE) method while the membranes containing large pores with tens of nanometers in diameter are prepared accordingly with the symmetric track-etch (TE) technique. Ionic conduction across the SE- and TE-membranes are studied under aqueous and aprotic electrolyte conditions. Scheme 1 shows the transport processes across the SE- and TE-PI membranes in aqueous and organic solutions. Membranes with single conical nanopores are also prepared by asymmetric etching of the ion tracks to better understand the different behavior of aqueous and aprotic electrolyte solutions from the corresponding changes in the current rectification. The use of single pore samples permits to discard possible effects related to the distribution of pore sizes found in multipore samples. In particular, the transition point at which the effective pore surface charge becomes zero is obtained from single nanopore electrical recordings in aprotic electrolyte solutions diluted with different mole fractions of water. This transition point provides information on the adsorption/desorption phenomena of the solvated metal ions on the pore surface.

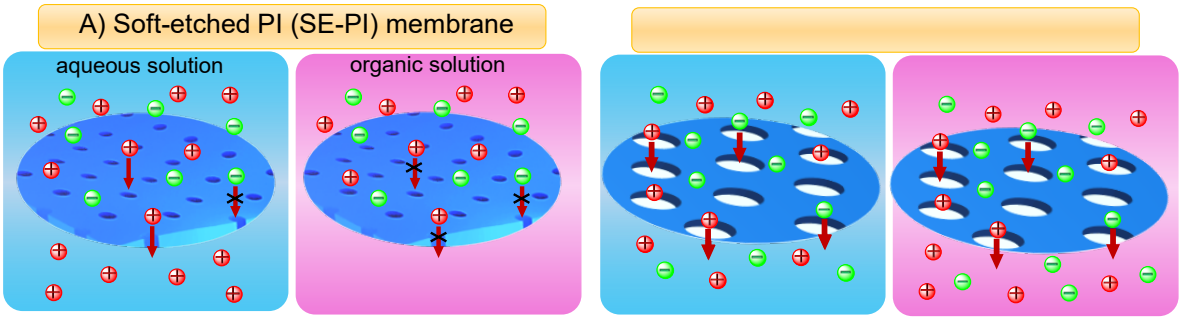

Scheme 1. Schematic view of the ion transport and rejection processes across soft-etched (SE) (A) and track-etched (TE) (B) PI-membranes in aqueous and organic solutions. The SE-PI membrane shows high selectivity in aqueous solution and low ionic current in organic solvent solutions. These effects are not so marked in the TE-PI membrane because of its large pore diameter.

2. Experimental

2.1. Materials

The chemicals and solvents used in this study include tetramethylammonium chloride (Me_4NCl), tetraethylammonium chloride (Et_4NCl), tetrapropylammonium chloride (Pr_4NCl), tetrabutylammonium chloride (Bu_4NCl), lithium perchlorate ($LiClO_4$), sodium perchlorate ($NaClO_4$), lithium bis(trifluoromethylsulphonyl)imide (LiTFSI), potassium hexafluorophosphate (KPF_6), anhydrous acetonitrile (ACN), anhydrous propylene carbonate (PC), and anhydrous dimethylformamide (DMF), which were obtained from Sigma-Aldrich, Schnelldorf, Germany, and used without any further treatment.

Polymer foils of polyimide (PI, Kapton50 HN, DuPont) and polyethylene terephthalate (PET, Hostaphan RN 12, Hoechst) of 12 μm thickness were irradiated with swift heavy ions (Au) of energy 11.4 MeV per nucleon at the linear accelerator UNILAC (GSI Helmholtzzentrum für Schwerionenforschung, Darmstadt, Germany). The polymer membranes with 10^9 and 10^3 ion tracks cm^{-2} were used together with single pore ion track membranes.

2.2. Fabrication of nanoporous membrane:

Before track etching, the ion tracks in polymer membranes were sensitized with UV light (320 nm) for 1 hr from both sides. For the fabrication of soft-etched (SE) nanopores, the ion tracks in the PI membrane (10^9 pores cm^{-2}) were selectively dissolved by soaking the sample in DMF solvent for ~20 h using previously reported techniques [17, 43].

The track-etched cylindrical nanopores in the PI membranes (10^3 pores/cm^2) were prepared with the symmetric track-etching technique. To this end, ion tracked PI membranes were immersed in a preheated etchant sodium hypochlorite (NaOCl, 13% active chlorine content) with constant stirring for 45 min. Moreover, the etchant temperature was maintained at 50°C with a circuit of heated water flowing through the double walls of the isothermal etching

bath. The single cylindrical nanopores in PET membranes were fabricated using a 2 M NaOH solution as etchant at 50°C [44].

The single conical nanopores in polymer membranes were fabricated through the asymmetric track-etching technique. Details of the single conical pore preparation in PI [18, 45] and PET membranes [21, 46] can be found elsewhere. The pore base diameter (*D*) was estimated under field emission scanning electron microscopy (FESEM) technique for the case of multipore membranes (Figure S1). The small pore opening diameter (*d*) was estimated using electrochemical techniques [45, 46]. Note however that the FESEM imaging of the subnanometer pores in the SE-PI membrane is exceedingly difficult because the charging of the sample at low resolution can deflect the scanning beam (Figure S1). However, we have considered previously the transport of quaternary ammonium ions and cationic metal-crown chelates and their corresponding current drops because of the pore blockage, thus suggesting that their nanoscale diameters are commensurate with the channel opening diameter [17].

The ion-tracked membranes samples were rinsed at least three times with deionized water and then immersed in water overnight to remove the residual salts before the current–voltage (*I–V*) measurements.

2.3. Current–voltage (I–V) curves

The electrical readouts of the soft-etched, track-etched and single-pore membranes were recorded with a Keithley 6487 picoammeter (Keithley Instruments, Cleveland, Ohio) under aqueous, aprotic organic solvents, and solvent/water mixed electrolyte solutions by fixing them in a home-made electrochemical cell [47, 48]. Electrolytes solutions were prepared for the different salts ($LiClO_4$, $NaClO_4$, LiTFSI and KPF_6) at 0.1 M concentration by dissolving them in water and in the anhydrous aprotic solvents. As an example, the bulk conductance of the 0.1M $LiClO_4$ electrolyte solution as a function of the aprotic solvent mole fraction in water is

shown in Figure S2. For the case of the nanoporous membrane, an effective membrane area of ~5 mm^2 was exposed to the electrolyte solution. Each chamber of the conductivity cell was filled with a maximum solution volume ~1.5 mL. To apply the input potentials and record the corresponding output currents, Ag|AgCl electrodes were dipped into the electrolyte solutions on both sides of the membrane [47, 48].

3. Results and discussion

The swift heavy ion tracks in the polymer membranes are comprised of the track core (highly damaged region of a few nanometers in diameter containing molecular fragments) [49] encompassed with the track halo (a region tens of nanometers in diameter with partially inter-connected polymer chains) [50]. Using the soft-etch technique, pores of a few nanometers in diameter are fabricated by selectively dissolving the track core with organic solvent [43]. The SE-PI membranes only allow the transport of alkali cations under aqueous conditions while they hinder the transport of divalent and alkylammonium cations as well as of cationic metal-crown ether complexes with molecular dimensions comparable with the nanopore diameter [17, 43].

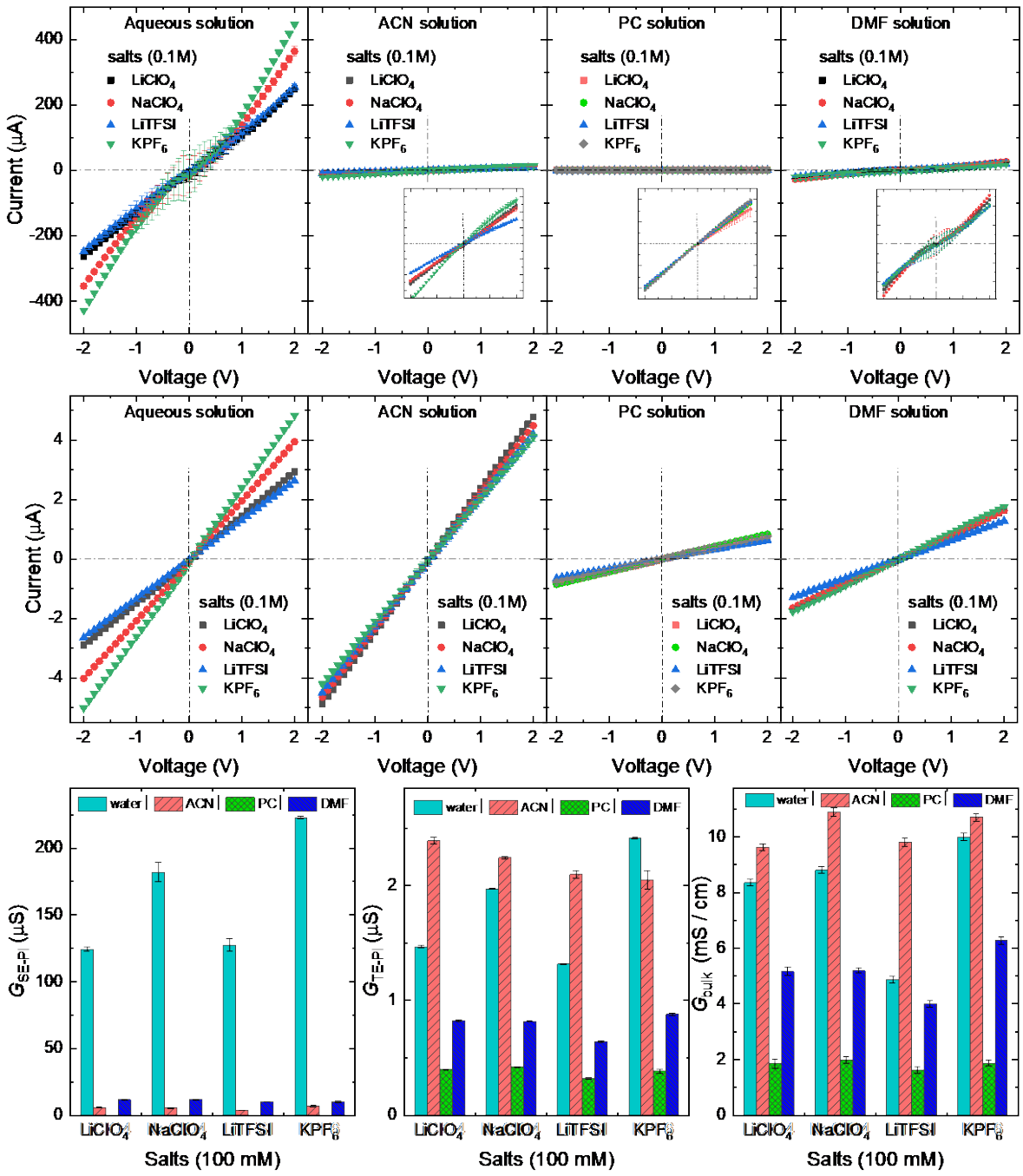

Figure 1. The *I–V* characteristics (i–iv) of soft-etched (SE)-PI multipore (10^9 pores cm^{-2}) membrane (A) and track-etched (TE)-PI multipore (10^3 pores cm^{-2}) membrane (B) measured in 0.1 M salt solutions obtained with water and anhydrous aprotic solvents such as acetonitrile, propylene carbonate and dimethylformamide. Changes in the conductance of the SE-PI membrane (C) and the TE-PI membrane (D) obtained from the corresponding *I–V* curves at voltage 2V. The respective bulk conductivities of the different 0.1 M salt solutions are shown for comparison (E). Note that in some cases, the error bars are smaller than the data point symbol size.

Figure 1 shows the current–voltage (*I–V*) curves of SE-PI membranes (10^9 pores cm^{-2}) and TE-PI membranes (10^3 pores cm^{-2}) measured in symmetric pure aqueous and anhydrous aprotic electrolytes. The 0.1 M salt solutions correspond to lithium perchlorate ($LiClO_4$), sodium perchlorate ($NaClO_4$), lithium bis(trifluoromethylsulphonyl)imide (LiTFSI), and potassium hexafluorophosphate (KPF_6). Under aqueous conditions, both SE- and TE-PI membranes exhibit high currents at positive and negative voltages due to the conduction of cations (Li^+, Na^+ and K^+) through the negatively charged nanopores, as shown in Figure 1 (see also Scheme 1). On the contrary, the *I–V* curves of organic electrolyte solutions show ionic currents across the SE-PI membrane that are much lower than the TE-PI membrane (Figure 1A and B(ii-iv). There are two plausible explanations for this dramatic drop in the ionic currents. It is well known that the solvation of alkali metal ions occurs in aprotic solvent molecules to give bulky cationic $[M–(solvent)_n]^+$ complexes [51-53]. Indeed, previous studies demonstrated that mainly four solvent molecules coordinate with a metal cation to form $[M–(solvent)_4]^+$ complexes in acetonitrile (ACN), propylene carbonate (PC) and dimethylformamide (DMF) [53-56]. For the case of anions, the interactions are very weak and thus anions remain uncoordinated in aprotic electrolytes due to the lack of hydrogen bonding [51, 56]. However, the anions are rather bulky and could be excluded from the pore solution because of the negative surface charge (Scheme 1). The strongly hindered conduction is then ascribed to the presence of bulky cationic species with hydrodynamic radii comparable or larger than the pore diameter. Alternatively, the pore surface could become positive due to the adsorption of cationic $[M–(solvent)_4]^+$ complexes [57]. Recently, Siwy and co-workers have successfully demonstrated experimentally and theoretically the switching of the pore charge from negative (aqueous solutions) to positive (PC electrolytes) in track-etched polymer nanopores and glass nanopipettes [28, 29]. In this case, the cationic species would be excluded electrostatically from the pore. Also, the anion passage across the membrane could be strongly hindered due to the

adsorbed metal-solvent complexes on the pore opening. For the case of TE-PI membranes, however, ions can easily pass through the large diameter pores.

For the sake of comparison, Figure 1(C,D) gives the membrane conductances obtained from the respective *I–V* curves of Figure 1(A,B). Figure 1C shows that the SE nanopore exhibits negligible membrane conductance in aprotic electrolytes compared to aqueous case. On the contrary, the TE-PI pores show significant membrane conductances in organic electrolytes (Figure 1D) that follow the bulk solution conductivities of the corresponding salts in Figure 1E.

To investigate further the effect of the aprotic solvent content on the ionic conduction, experiments have also been conducted in electrolyte solutions having different solvent molar fractions ($\chi_{solvent}$). To this end, mixtures of the above aprotic solvents with water are considered in the range between $\chi_{solvent} = 0$ (pure water) and $\chi_{solvent} = 1$ (pure solvent) at constant 0.1 M $LiClO_4$ solution concentration.

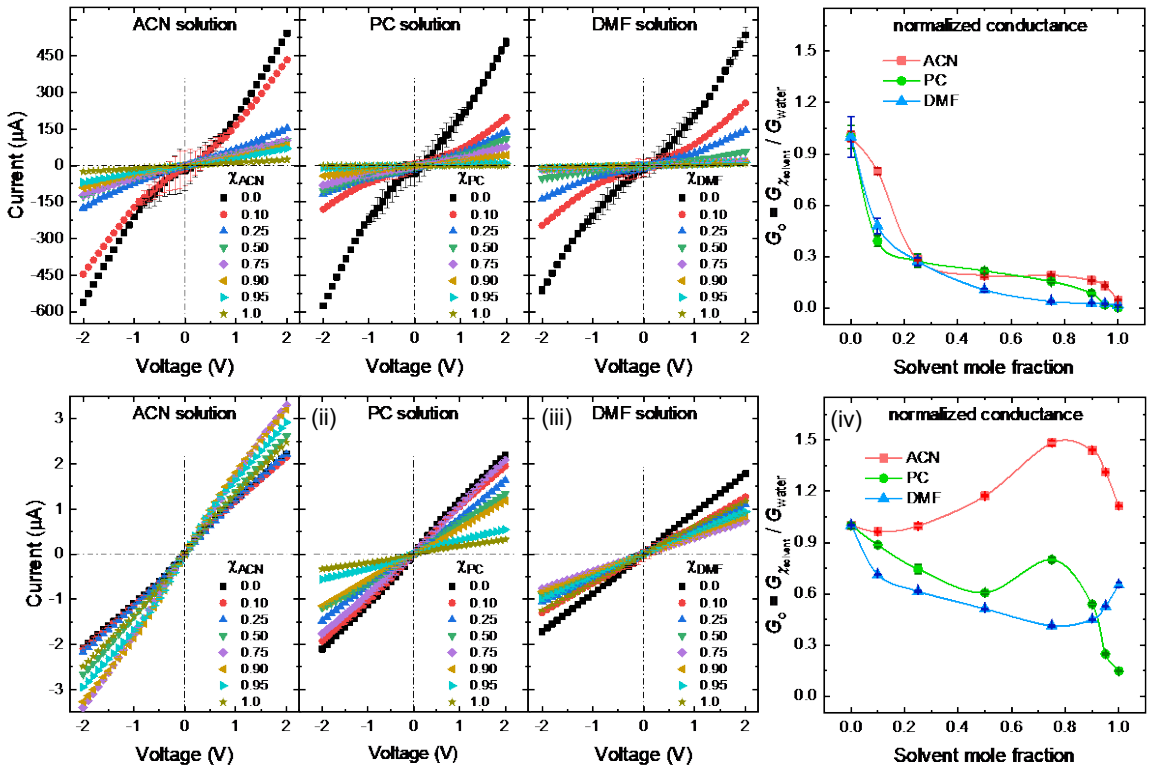

Figure 2. The *I–V* characteristics (i–iii) and normalized conductances (iv) for the SE multipore (10^9 pores cm^{-2}) PI-membrane (A) and the TE multipore (10^3 pores cm^{-2}) PI-membrane (B) in 0.1M $LiClO_4$

electrolyte solution at different aprotic solvent mole fractions in water. Note that in some cases, the error bars are smaller than the data point symbol size.

Figure 2 shows the *I–V* characteristics and dimensionless conductances, normalized to that of water, of the SE- and TE-PI multipore membranes for different solvent mole fractions. For the case of the SE-PI membrane and the ACN solvent, a conductance decrease of only ~21% is obtained upon dilution to $\chi_{solvent} = 0.1$. On the contrary, conductance decreases of ~61% and 53% are obtained for the PC and DMF solvents, respectively. Eventually, at $\chi_{solvent} > 0.25$, ionic conduction is almost blocked. The conductance drops obtained in Figure 2A by replacing water with organic solvents can be due to the solvation of metal ions. The resulting solvated metal ion, $[M–(solvent)_4]^+$, should diffuse slowly through the nanopores and could also be adsorbed on the pore surface, contributing further to the ionic hindrance in the SE-PI membrane. On the contrary, no significant conductance decrease for $\chi_{solvent} \geq 0.25$ is noted for the TE-PI membrane, as shown in Figure 2B. In this case, the membrane conductance changes follow those of the bulk solution conductance (Figure S2), suggesting that the ionic transport through the track-etched nanopores occurs without significant hindrance. Note that, for the case of the ACN solvent, an increase in membrane conductance is obtained by gradually reducing water concentration in the 0.1 M $LiClO_4$ solution compared to the case of the PC and DMF solvents. Note that the track-etching of PI membrane under symmetric conditions for shorter time (< 1 h) leads to the fabrication of hourglass shaped (biconical) nanopores [58] instead of cylindrical nanopores with surface opening size of ~420 ± 30 nm (Figure S1) and inner opening diameter of tens of nanometers. On the contrary, the cylindrical shaped nanopores (diameter > 20 nm) in the PET membrane can be fabricated successfully [44]. Figure S3 shows that even the narrow cylindrical nanopores (~20 nm obtained for the case of 4 min etch time) exhibit high conductances in ACN electrolytes compared to the aqueous ones.

These findings suggest that significant pore blocking occurs in the SE-pores due to the ionic hindrance and possible adsorption of the solvated metal cations on the pore surface.

To elucidate the role of surface pore charges, we have conducted additional experiments with single conical nanopores. These negatively charged asymmetric nanopores rectify the ionic current and minor changes in the pore charges and/or effective diameter are directly transduced in an electronic readout. Figure 3 shows the *I–V* curves of the PI single conical nanopore recorded in 0.1M electrolyte solutions of different salts in pure water and anhydrous solvents, separately. Under aqueous conditions, the deprotonation of carboxylic acid groups gives a negatively charged conical nanopore that exhibits current rectification due to the preferential cationic conduction from the tip to the base opening of the conical pore (Figure 3B). However, a different behavior is observed for aprotic organic solvents (Figures 3C-E): the conical pore becomes anion- rather than cation-selective in the PC electrolyte, as shown by the inverted current rectification, suggesting now a positively charged pore. In this case, the pore chemical moieties (carboxylic acid groups) are not ionized because of the relatively low dielectric constant of the organic solvents compared to that of water. It is the solvated metal ion $[M–(PC)_4]^+$ that adheres to the pore surface, resulting in the inversion of current rectification. Figure 3C shows that this inversion does not depend on the type of anion or cation in the PC electrolyte.

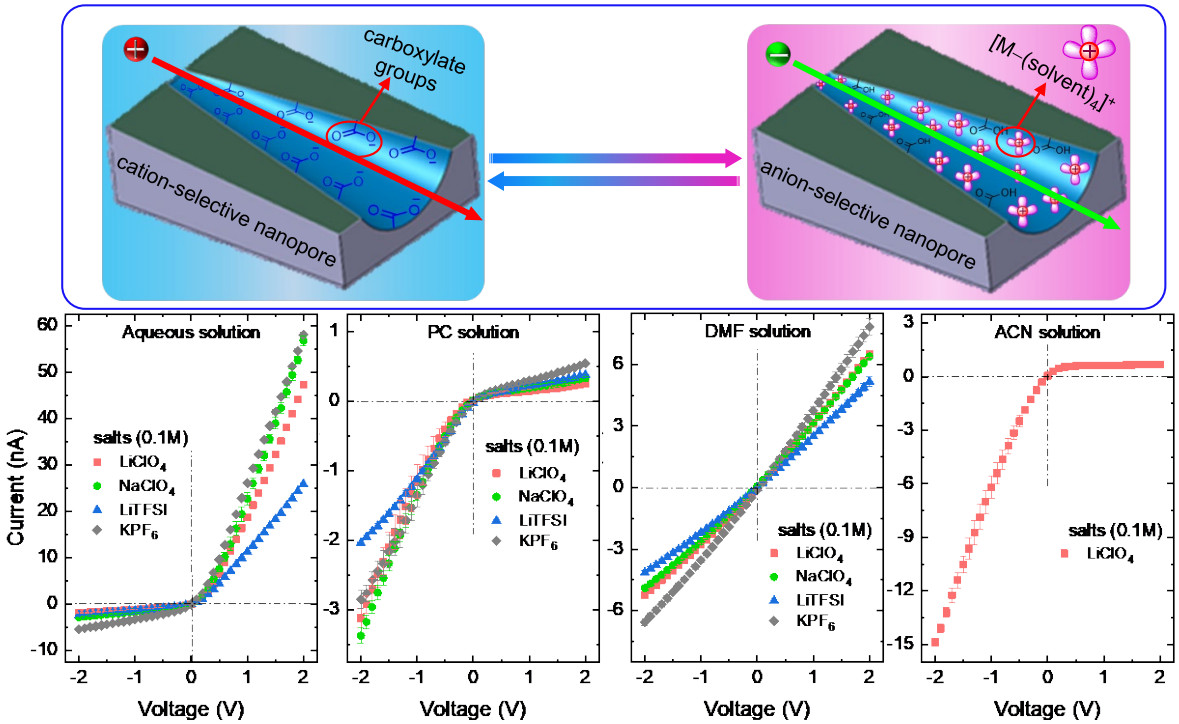

Figure 3. Scheme of the surface charge and ionic conduction in single conical nanopores immersed in aqueous and organic solutions (A). The *I–V* curves obtained with the PI single conical nanopore (approximate diameters are $d \sim 37 \pm 5$ nm and $D \sim 850 \pm 20$ nm) in 0.1M solutions of different salts prepared in water (B), propylene carbonate (C), dimethylformamide (D) and acetonitrile (E). Note that in some cases, the error bars are smaller than the data point symbol size.

Note also that the rectified ion currents in the PC electrolytes are lower than those of the corresponding aqueous electrolytes because of the lower bulk solution conductivities. Previous studies have confirmed this inversion of current rectification when the surface charge is changed from negative to positive by the functionalization of the pore surface with cationic moieties [45, 59-62]. Recently, Siwy and coworkers have also shown that in PC salt solutions, the surface charge of conical nanopores in polycarbonate and polyethylene terephthalate (PET) membranes, together with the case of glass nanopipettes, switched from negative to positive because of the adsorption of $[M–(PC)_4]^+$ complexes on the pore surface [28, 29]. On the contrary, we have not noticed this inverse rectification when the PI conical nanopore is exposed to salt solutions prepared in the anhydrous DMF solvent (Figure 3D). This fact would suggest

that the concentration of adsorbed $[M–(DMF)_4]^+$ complexes on the pore surface is not enough to impart the net positive charge required for the rectification inversion. This result could be related to the presence of moisture adsorbed by DMF from the atmosphere, which in turn generates negative charges due to deprotonation of pore surface carboxylate groups. Yin *et al*. have reported the influence of the water content in DMF solutions on the current rectification of glass nanopipettes [30]. For the case of the ACN solvent, we have observed a strong rectification inversion in 0.1M $LiClO_4$ electrolyte solutions, as shown in Figure 3E. However, we were unable to conduct the *I–V* measurements with other salts because of the limited chemical stability of the PI nanopore in acetonitrile solutions. Figure S4 shows that the PI nanopore exhibits stable current rectification over several cycles in PC electrolytes. On the contrary, the ion current is stable only for a few cycles in the case of ACN electrolytes. The observed increase of ion current with time may suggest the deformation of the pore tip opening in this case. Therefore, further experiments with the PI single pore were conducted only for PC electrolyte solutions.

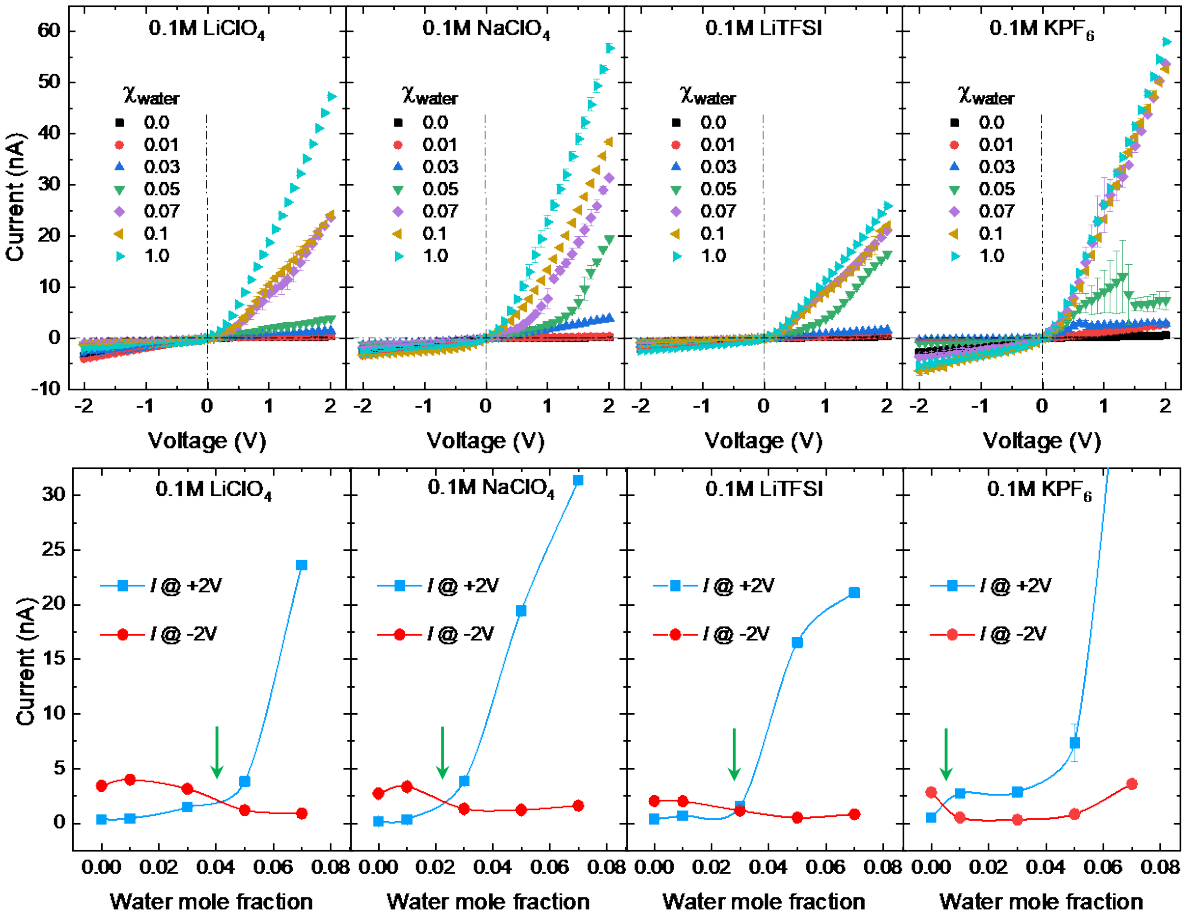

Figure 4. The *I*–*V* curves of the PI single conical pore (approximate diameters are $d \sim 30 \pm 5$ nm and $D \sim 1030 \pm 20$ nm) immersed in 0.1M electrolyte solutions of salts at different mole fractions of water in propylene carbonate solution (A). The rectified ion currents at +2 V (blue points) and −2 V (red points) obtained from the corresponding *I*–*V* curves (B). The arrow at the intersection line gives the transition point at which the pore charge is switched from positive to negative. Note that in some cases, the error bars are smaller than the data point symbol size.

To elucidate the aqueous-sensitive adsorption/desorption capability of the $[M–(PC)_4]^+$ complexes on the pore surface, we have conducted also experiments with different water mole fractions from $\chi_{water} = 0$ (anhydrous PC solution) to $\chi_{water} = 1$ (pure aqueous solution). Figure 4A shows the *I*–*V* curves of the PI single conical nanopore in contact with different salts in the PC solvent at different mole fractions of water. Upon increasing the water mole fraction, the *I*–*V* curves gradually flipped to the normal current rectification case due to the displacement of the adsorbed $[M–(PC)_4]^+$ complexes by the water molecules. As mentioned above, the presence

of water in the electrolyte disrupts the adsorbed layer of $[M–(PC)_4]^+$ cations in the pore surface and triggers the ionization of the carboxylate groups. Thus, the pore conducts alkali cations rather than anions.

The desorption of the different cations $[M–(PC)_4]^+$ from the pore surface depends on the type of salt solution and the χ_{water} values. Figure 4B shows the changes observed in the rectified ion currents at voltages +2 V and –2 V as a function of the water mole fraction. As χ_{water} increases, the interface between the PC solvent and the pore surface changes [57], giving gradual current increases and decreases at positive and negative voltages, respectively. Eventually, at a given χ_{water} level the negative and positive currents are equal. Thus, a transition point is reached at which the net surface charge is zero and the conical nanopore exhibits ohmic behavior. Below the transition point, the $[M–(PC)_4]^+$ cations adsorbed on the nanopore surface impart a net positive charge to the pore but when the water content exceeds this point, the carboxylic acid deprotonation gives a negative pore. The transition point of the different salts can be obtained from Figure 4B. For the case of $LiClO_4$, the transition point is reached at χ_{water} = 0.04, suggesting that a minimum ~4% of water content in the PC electrolyte is required to detach the $[Li–(PC)_4]^+$ species from the pore surface. This result is consistent with the previously reported value of ~5% water content in the PC electrolyte and single polycarbonate nanopore [29]. For $NaClO_4$ and LiTFSI salts, this transition point is obtained at χ_{water} = 0.023 and χ_{water} = 0.03, respectively. For the case of KPF_6 salt, however, the transition point is reached at very low water content, χ_{water} = 0.004 (< 0.4%), which is required to dissociate the $[K–(PC)_4]^+$ cation from the pore surface. Moreover, two conductance levels of the nanopore are found for the case of the PF_6^- anion (Figures 4A(iv) and S5). Recently, we have given a detailed account of the negative differential resistance (NDR) effect for the case of the F^- ion at low concentrations [63]. Fluoride ions show a high hydration energy, can have a second hydration

shell, and tend to strongly immobilize the surrounding water molecules, especially in nanoscale environments. We suspect that fluoride pore entrance affects the free water pore networks available for ionic conduction. According to this interpretation, no NDR should be apparent for wide nanopore openings where the charge concentration is small as observed experimentally and discussed theoretically in the above reference. This mechanism could also be present in the case of the PF_6^- anion when the applied potential exceeded the threshold voltage. Although the total concentration of KPF_6 used here (100 mM) is higher than that of the KF solution [63], the NDR behavior is observed upon exposure to aprotic electrolyte solution containing 2% to 5% water content only and vanishes in electrolyte solutions with > 7% water content (Figure S5). Additional experiments not shown here reveal that conical nanopores exposed to aqueous solutions of KPF_6 in the mM range show indeed the NDR phenomenon. This fact supports our previous finding that the water dissolved PF_6^- anion concentration is in the range responsible for the nanopore NDR and threshold-switching characteristics.

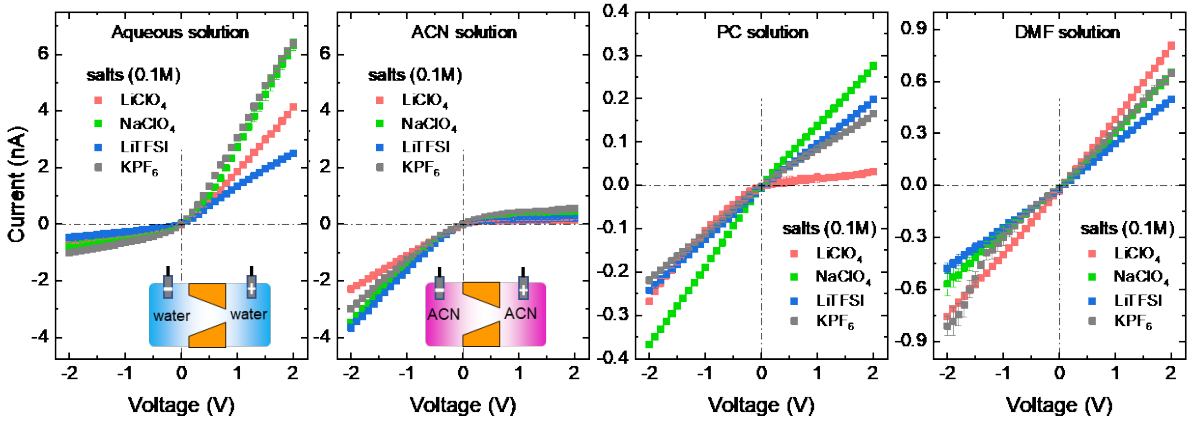

Figure 5. The *I–V* curves obtained with the PET single conical nanopore (approximate diameters are *d* ~ 23 ± 5 nm and *D* ~ 590 ± 30 nm) in 0.1M salt solutions for water (A), acetonitrile (B), propylene carbonate (C) and dimethylformamide (D) solvents. Note that in some cases, the error bars are smaller than the data point symbol size

We have also conducted experiments with the PET single conical nanopore using the same set of salt solutions and aprotic solvents (Figures 5A-D). The PET single conical nanopore

exhibits inverse current rectification similar to PI nanopores, which shows an effective positive pore charge due to the adsorption of solvated metal ion species also on the PET surface. Again, no rectification inversion is noticed in DMF electrolyte solutions, i.e., the ionic conduction is similar to that seen in the PI nanopore. Figures 5B and 5C show that the PET nanopore exhibits higher current rectification inversion in the ACN solutions than in the PC solutions. This result could be due to the high bulk conductivities of the salt solutions in the ACN solvent. Note also that both the PI and PET single pores show rectification inversion in salt solutions prepared in the PC and ACN solvents. This fact suggests again that the water content in the PC and ACN solvents is much lower than that of the commercial DMF solvent (Figure 5D).

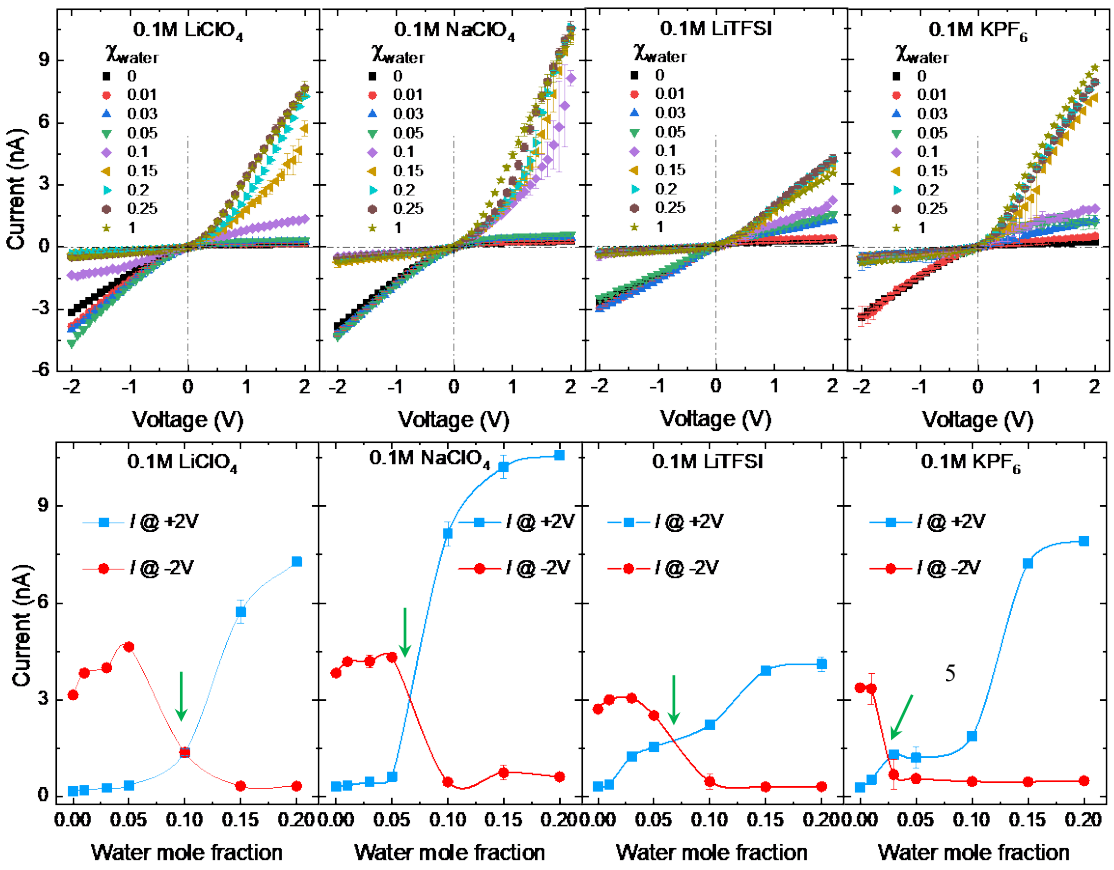

Figure 6. The *I–V* curves of PET single conical nanopore (approximate diameters are $d \sim 20 \pm 3$ nm and $D \sim 870 \pm 30$ nm) in 0.1M electrolyte solutions of different salts and water mole fractions in acetonitrile solution (A). The rectified ion current at +2 V (blue points) and –2 V (red points) obtained from the corresponding *I–V* curves (B). The arrow at the intersection line represents the transition point

at which the pore charge changes from positive to negative. Note that in some cases, the error bars are smaller than the data point symbol size

The transition point of the PI nanopore was successfully obtained in PC solutions of different water mole fractions but not for the ACN solvent due to the limited electrolyte stability. Contrary to the case of the PI nanopore, however, the PET single conical nanopore exhibits chemical robustness in ACN solvent. Therefore, additional experiments are conducted with the PET nanopore to determine the transition point in ACN salt solutions. Figure 6A shows the *I–V* curves of the PET nanopore for different water mole fractions. The rectification inversion (high currents at negative voltages) gradually vanishes with the increase of the water content in the ACN electrolyte because of the increased carboxylic acid dissociation in the pore. Figure 6B shows the transition point at which the pore net charge becomes zero at voltages +2 V and −2 V, which is obtained by diluting the electrolyte with different water mole fractions χ_{water}.

Note that the water content required for the transition point of the ACN solution (Figure 6B) is almost doubled compared to that of PC solutions (Figure 4B). For the case of $LiClO_4$, the transition point increases from χ_{water} = ~0.04 (PC solution) to χ_{water} = ~0.1 (ACN solution). Similarly, for the $NaClO_4$ solution this point increases from χ_{water} = ~0.023 to χ_{water} = ~0.065 and for the LiTFSI from ~0.03 to ~0.067 (PC solution). For the case of KPF_6, however, there is a six times increase, from ~0.004 to ~0.025, in the transition point. Also, it is observed that the $[M–(ACN)_4]^+$ complex is more tightly bound to the pore surface than the $[M–(PC)_4]^+$ complex because in the first case a higher water content in the electrolyte solution is required to dissociate the solvated metal ion from the pore surface.

Moreover, the ion transport of PET single conical nanopore is also investigated under asymmetric electrolyte conditions. To this end, salt solutions prepared in aqueous and ACN

solvent are considered because of their comparable bulk solution conductivities. Figure S6 shows the comparison of the *I–V* curves when the pore is exposed to symmetric and asymmetric electrolyte conditions. For this purpose, the salts solution prepared in water is placed on tip side of the conical nanopore, while the base side of the pore contain the ACN solution and *vice versa*. It is well known that in conical nanopores, the electrically charged tip region mainly dictates the ion transport across the membrane. The pore tip charge polarity is switched from negative to positive when the aqueous solution is replaced with ACN solution as evidenced from the *I–V* characteristics of Figure S6. Due to the opposite polarity of the surface charges in the tip and base sides of the conical nanopore, it exhibits a diode behavior under water/ACN electrolyte conditions.

To compare the effects of cation type (alkali or ammonium) on the single pore conduction, experiments have also been conducted in tetraalkylammonium salts (R_4NCl). Contrary to alkali salts, the pore does not show rectification inversion in R_4NCl (Figures S7 and S8), suggesting that solvated R_4N cations could not adsorb on the pore surface. It has been mentioned that the solvation of R_4N^+ cation in aprotic solvents occurs with very weak ion-dipole interaction [64] because the positive charge is localized on the nitrogen atom surrounded by four alkyl chains in this case. Thus, these salts mainly form ion pairs and continuums in organic solvents [65].

4. Conclusions

In summary, we have described ionic conduction phenomena in multipore and single conical pore membranes under aqueous and aprotic electrolyte conditions. Under aprotic electrolyte conditions, the soft-etched membrane with pores having a few nanometers in diameter show conductances that dramatically decrease with the formation of $[M–(solvent)_4]^+$ cations causing pore hindrance. On the contrary, the conductance of the track-etched membrane

having pore diameters in the tens of nanometers range follows the same trend of the corresponding bulk solution conductivities.

The different effective pore charges observed in pure aqueous, aprotic, and water/solvent mixed electrolytes have been identified from the changes in the current rectification of single conical nanopores. For the case of the PC and ACN electrolytes, the conical pore exhibited ion current rectification inversion due to the adsorption of solvated metal cations $[M–(PC)_4]^+$ and $[M–(ACN)_4]^+$ on the pore surface. Moreover, ionic conduction in aprotic electrolytes with different water mole fractions showed that the amount of water for the transition point of the single pore in ACN electrolyte is almost twice as much as that obtained in the PC electrolyte, which suggests that the $[M–(ACN)_4]^+$ cation was tightly attached to the pore walls. These findings should be useful for membrane-based molecular filtration, separation, and purification processes in organic solvents, especially in pharmaceutical industries, as well as in energy storage nanofluidic devices operating in organic solvents.

Acknowledgements

S.N., M.A., K.F. and W.E. acknowledge the support from the LOEWE project iNAPO, Hessen State Ministry of Higher Education, Research and the Arts, Germany. P.R., J. C., and S. M. acknowledge the funding from project PGC2018-097359-B-I00, Ministry of Science and Innovation and FEDER. The authors are thankful to Prof. C. Trautmann and Dr. M. E. Toimil Molares (GSI, Material Research Department) for their support with the heavy ion irradiation experiments, and Dr. M. Wagner for his help in FESEM imaging analysis. The heavy ion irradiation is based on a UMAT experiment, which was performed at the X0-beamline of the UNILAC at the GSI Helmholtzzentrum für Schwerionenforschung, Darmstadt (Germany) in the frame of FAIR Phase-0.

References

[1] M. Belaya, V. Levadny, D.A. Pink, Electric Double Layer near Soft Permeable Interfaces. 1. Local Electrostatic, Langmuir, 10 (1994) 2010-2014.
[2] B. Hille, Ion channels of excitable membranes, Third ed., Sinauer Associates Inc., USA, 2001.
[3] T. Ma, J.-M. Janot, S. Balme, Track-Etched Nanopore/Membrane: From Fundamental to Applications, Small Methods, 4 (2020) 2000366.
[4] J. Zhang, K. Zhan, S. Wang, X. Hou, Soft interface design for electrokinetic energy conversion, Soft Matter, 16 (2020) 2915-2927.
[5] R.P. Buck, Kinetics of bulk and interfacial ionic motion: microscopic bases and limits for the nernst-planck equation applied to membrane systems, J. Membr. Sci., 17 (1984) 1-62.
[6] G. Trefalt, S.H. Behrens, M. Borkovec, Charge Regulation in the Electrical Double Layer: Ion Adsorption and Surface Interactions, Langmuir, 32 (2016) 380-400.
[7] F.B. van Swol, D.N. Petsev, Solution Structure Effects on the Properties of Electric Double Layers with Surface Charge Regulation Assessed by Density Functional Theory, Langmuir, 34 (2018) 13808-13820.
[8] S. Balme, T. Ma, E. Balanzat, J.-M. Janot, Large osmotic energy harvesting from functionalized conical nanopore suitable for membrane applications, J. Membr. Sci., 544 (2017) 18-24.
[9] H. Bayley, P.S. Cremer, Stochastic sensors inspired by biology, Nature, 413 (2001) 226-230.
[10] S. Howorka, Z. Siwy, Nanopore analytics: sensing of single molecules, Chem. Soc. Rev., 38 (2009) 2360-2384.
[11] Z.S. Siwy, S. Howorka, Engineered voltage-responsive nanopores, Chem. Soc. Rev., 39 (2010) 1115-1132.
[12] C. Dekker, Solid-state nanopores, Nat. Nanotechnol., 2 (2007) 209-215.
[13] X. Hou, Smart Gating Multi-Scale Pore/Channel-Based Membranes, Adv. Mater., 28 (2016) 7049-7064.
[14] P. Ramirez, J. Cervera, M. Ali, S. Nasir, W. Ensinger, S. Mafe, Impact of Surface Charge Directionality on Membrane Potential in Multi-ionic Systems, J. Phys. Chem. Lett., 11 (2020) 2530-2534.
[15] N.I. Shtanko, V.Y. Kabanov, P.Y. Apel, M. Yoshida, A.I. Vilenskii, Preparation of permeability-controlled track membranes on the basis of 'smart' polymers, J. Membr. Sci., 179 (2000) 155-161.
[16] M. Ali, I. Ahmed, P. Ramirez, S. Nasir, C.M. Niemeyer, S. Mafe, W. Ensinger, Label-Free Pyrophosphate Recognition with Functionalized Asymmetric Nanopores, Small, 12 (2016) 2014-2021.
[17] M. Ali, S. Nasir, K. Froehlich, P. Ramirez, J. Cervera, S. Mafe, W. Ensinger, Size-Based Cationic Molecular Sieving through Solid-State Nanochannels, Adv. Mater. Interfaces, 8 (2021) 2001766.
[18] M. Ali, R. Neumann, W. Ensinger, Sequence-Specific Recognition of DNA Oligomer Using Peptide Nucleic Acid (PNA)-Modified Synthetic Ion Channels: PNA/DNA Hybridization in Nanoconfined Environment, ACS Nano, 4 (2010) 7267-7274.
[19] R. Duan, F. Xia, L. Jiang, Constructing Tunable Nanopores and Their Application in Drug Delivery, ACS Nano, 7 (2013) 8344-8349.
[20] X. Hou, W. Guo, L. Jiang, Biomimetic smart nanopores and nanochannels, Chem. Soc. Rev., 40 (2011) 2385-2401.
[21] S. Nasir, M. Ali, I. Ahmed, C.M. Niemeyer, W. Ensinger, Phosphoprotein Detection with a Single Nanofluidic Diode Decorated with Zinc Chelates, ChemPlusChem, 85 (2020) 587-594.
[22] G. Pérez-Mitta, M.E. Toimil-Molares, C. Trautmann, W.A. Marmisollé, O. Azzaroni, Molecular Design of Solid-State Nanopores: Fundamental Concepts and Applications, Adv. Mater., (2019) 1901483.
[23] I. Duznovic, M. Diefenbach, M. Ali, T. Stein, M. Biesalski, W. Ensinger, Automated measuring of mass transport through synthetic nanochannels functionalized with polyelectrolyte porous networks, J. Membr. Sci., 591 (2019) 117344.
[24] P. Ramirez, J. Cervera, V. Gomez, M. Ali, S. Nasir, W. Ensinger, S. Mafe, Membrane potential of single asymmetric nanopores: Divalent cations and salt mixtures, J. Membr. Sci., 573 (2019) 579-587.
[25] I.V. Blonskaya, N.E. Lizunov, K. Olejniczak, O.L. Orelovich, Y. Yamauchi, M.E. Toimil-Molares, C. Trautmann, P.Y. Apel, Elucidating the roles of diffusion and osmotic flow in controlling

the geometry of nanochannels in asymmetric track-etched membranes, J. Membr. Sci., 618 (2021) 118657.
[26] T. Ma, E. Balanzat, J.-M. Janot, S. Balme, Single conical track-etched nanopore for a free-label detection of OSCS contaminants in heparin, Biosens. Bioelectron., 137 (2019) 207-212.
[27] M. Davenport, A. Rodriguez, K.J. Shea, Z.S. Siwy, Squeezing Ionic Liquids through Nanopores, Nano Lett., 9 (2009) 2125-2128.
[28] R.A. Lucas, C.-Y. Lin, Z.S. Siwy, Electrokinetic Phenomena in Organic Solvents, J. Phys. Chem. B, 123 (2019) 6123-6131.
[29] T. Plett, W. Shi, Y. Zeng, W. Mann, I. Vlassiouk, L.A. Baker, Z.S. Siwy, Rectification of nanopores in aprotic solvents – transport properties of nanopores with surface dipoles, Nanoscale, 7 (2015) 19080-19091.
[30] X. Yin, S. Zhang, Y. Dong, S. Liu, J. Gu, Y. Chen, X. Zhang, X. Zhang, Y. Shao, Ionic Current Rectification in Organic Solutions with Quartz Nanopipettes, Anal. Chem., 87 (2015) 9070-9077.
[31] T.-J. Chou, A. Tanioka, Ionic behavior across charged membranes in methanol–water solutions. I: Membrane potential, J. Membr. Sci., 144 (1998) 275-284.
[32] C.H. Hamann, V. Theile, S. Koter, Transport properties of cation-exchange membranes in aqueous and methanolic solutions. Diffusion and osmosis, J. Membr. Sci., 78 (1993) 147-153.
[33] G.B. Westermann-Clark, C.C. Christoforou, Note on nonaqueous electrokinetic transport in charged porous media, J. Membr. Sci., 20 (1984) 325-338.
[34] J. Barthel, H.-J. Gores, G. Schmeer, R. Wachter, Non-aqueous electrolyte solutions in chemistry and modern technology, Springer Berlin Heidelberg, Berlin, Heidelberg, 1983, pp. 33-144.
[35] P. Marchetti, M.F. Jimenez Solomon, G. Szekely, A.G. Livingston, Molecular Separation with Organic Solvent Nanofiltration: A Critical Review, Chem. Rev., 114 (2014) 10735-10806.
[36] C. Liu, G. Dong, T. Tsuru, H. Matsuyama, Organic solvent reverse osmosis membranes for organic liquid mixture separation: A review, J. Membr. Sci., 620 (2021) 118882.
[37] Y. Yan, L. He, Y. Li, D. Tian, X. Zhang, K. Liu, L. Jiang, Unidirectional liquid transportation and selective permeation for oil/water separation on a gradient nanowire structured surface, J. Membr. Sci., 582 (2019) 246-253.
[38] J. Vatamanu, Z. Hu, D. Bedrov, C. Perez, Y. Gogotsi, Increasing Energy Storage in Electrochemical Capacitors with Ionic Liquid Electrolytes and Nanostructured Carbon Electrodes, J. Phys. Chem. Lett., 4 (2013) 2829-2837.
[39] P. Simon, Y. Gogotsi, Materials for electrochemical capacitors, Nat. Mater., 7 (2008) 845-854.
[40] K. Xu, Nonaqueous Liquid Electrolytes for Lithium-Based Rechargeable Batteries, Chem. Rev., 104 (2004) 4303-4418.
[41] A. Manthiram, X. Yu, S. Wang, Lithium battery chemistries enabled by solid-state electrolytes, Nat. Rev. Mater., 2 (2017) 16103.
[42] Y. Xie, H. Zou, H. Xiang, R. Xia, D. Liang, P. Shi, S. Dai, H. Wang, Enhancement on the wettability of lithium battery separator toward nonaqueous electrolytes, J. Membr. Sci., 503 (2016) 25-30.
[43] K. Froehlich, S. Nasir, M. Ali, P. Ramirez, J. Cervera, S. Mafe, W. Ensinger, Fabrication of soft-etched nanoporous polyimide membranes for ionic conduction and discrimination, J. Membr. Sci., 617 (2021) 118633.
[44] Q.H. Nguyen, M. Ali, V. Bayer, R. Neumann, W. Ensinger, Charge-selective transport of organic and protein analytes through synthetic nanochannels, Nanotechnology, 21 (2010) 365701.
[45] M. Ali, B. Schiedt, K. Healy, R. Neumann, W. Ensinger, Modifying the surface charge of single track-etched conical nanopores in polyimide, Nanotechnology, 19 (2008) 085713.
[46] P.Y. Apel, Y.E. Korchev, Z. Siwy, R. Spohr, M. Yoshida, Diode-Like Single-Ion Track Membrane Prepared by Electro-Stopping, Nucl. Instrum. Methods Phys. Res., Sect. B, 184 (2001) 337-346.
[47] P. Ramirez, J. Cervera, V. Gomez, M. Ali, S. Nasir, W. Ensinger, S. Mafe, Optimizing Energy Transduction of Fluctuating Signals with Nanofluidic Diodes and Load Capacitors, Small, 14 (2018).
[48] P. Ramirez, V. Garcia-Morales, V. Gomez, M. Ali, S. Nasir, W. Ensinger, S. Mafe, Hybrid Circuits with Nanofluidic Diodes and Load Capacitors, Phys. Rev. Applied, 7 (2017) 064035.
[49] P.Y. Apel, I.V. Blonskaya, T.W. Cornelius, R. Neumann, R. Spohr, K. Schwartz, V.A. Skuratov, C. Trautmann, Influence of temperature during irradiation on the structure of latent track in polycarbonate, Radiat. Meas., 44 (2009) 759-762.

[50] D. Schauries, P. Mota-Santiago, E.P. Gilbert, N. Kirby, C. Trautmann, P. Kluth, Structure, morphology and annealing behavior of ion tracks in polycarbonate, Eur. Polymer J., 108 (2018) 406-411.
[51] D.M. Seo, O. Borodin, S.-D. Han, P.D. Boyle, W.A. Henderson, Electrolyte Solvation and Ionic Association II. Acetonitrile-Lithium Salt Mixtures: Highly Dissociated Salts, J. Electrochem. Soc., 159 (2012) A1489-A1500.
[52] D. Spångberg, K. Hermansson, The solvation of Li+ and Na+ in acetonitrile from ab initio-derived many-body ion–solvent potentials, Chem. Phys., 300 (2004) 165-176.
[53] S. Amara, J. Toulc'Hoat, L. Timperman, A. Biller, H. Galiano, C. Marcel, M. Ledigabel, M. Anouti, Comparative Study of Alkali-Cation-Based (Li+, Na+, K+) Electrolytes in Acetonitrile and Alkylcarbonates, ChemPhysChem, 20 (2019) 581-594.
[54] J. Barthel, R. Buchner, E. Wismeth, FTIR Spectroscopy of Ion Solvation of LiClO4 and LiSCN in Acetonitrile, Benzonitrile, and Propylene Carbonate, J. Solution Chem., 29 (2000) 937-954.
[55] K. Fujii, H. Wakamatsu, Y. Todorov, N. Yoshimoto, M. Morita, Structural and Electrochemical Properties of Li Ion Solvation Complexes in the Salt-Concentrated Electrolytes Using an Aprotic Donor Solvent, N,N-Dimethylformamide, J. Phys. Chem. C, 120 (2016) 17196-17204.
[56] S. Hwang, D.-H. Kim, J.H. Shin, J.E. Jang, K.H. Ahn, C. Lee, H. Lee, Ionic Conduction and Solution Structure in LiPF6 and LiBF4 Propylene Carbonate Electrolytes, J. Phys. Chem. C, 122 (2018) 19438-19446.
[57] H. Liu, Y. Tong, N. Kuwata, M. Osawa, J. Kawamura, S. Ye, Adsorption of Propylene Carbonate (PC) on the LiCoO2 Surface Investigated by Nonlinear Vibrational Spectroscopy, J. Phys. Chem. C, 113 (2009) 20531-20534.
[58] L. Lin, J. Yan, J. Li, Small-Molecule Triggered Cascade Enzymatic Catalysis in Hour-Glass Shaped Nanochannel Reactor for Glucose Monitoring, Anal. Chem., 86 (2014) 10546-10551.
[59] M. Ali, P. Ramirez, S. Mafe, R. Neumann, W. Ensinger, A pH-Tunable Nanofluidic Diode with a Broad Range of Rectifying Properties, ACS Nano, 3 (2009) 603-608.
[60] P. Ramirez, J.A. Manzanares, J. Cervera, V. Gomez, M. Ali, I. Pause, W. Ensinger, S. Mafe, Nanopore charge inversion and current-voltage curves in mixtures of asymmetric electrolytes, J. Membr. Sci., 563 (2018) 633-642.
[61] M. Lepoitevin, B. Jamilloux, M. Bechelany, E. Balanzat, J.-M. Janot, S. Balme, Fast and reversible functionalization of a single nanopore based on layer-by-layer polyelectrolyte self-assembly for tuning current rectification and designing sensors, RSC Adv., 6 (2016) 32228-32233.
[62] C.-Y. Lin, T. Ma, Z.S. Siwy, S. Balme, J.-P. Hsu, Tunable Current Rectification and Selectivity Demonstrated in Nanofluidic Diodes through Kinetic Functionalization, J. Phys. Chem. Lett., 11 (2020) 60-66.
[63] P. Ramirez, J.J. Perez-Grau, J. Cervera, S. Nasir, M. Ali, W. Ensinger, S. Mafe, Negative differential resistance and threshold-switching in conical nanopores with KF solutions, Appl. Phys. Lett., 118 (2021) 181903.
[64] Y. Marcus, Tetraalkylammonium Ions in Aqueous and Non-aqueous Solutions, J. Solution Chem., 37 (2008) 1071-1098.
[65] T. Takamuku, M. Yamamoto, T. To, M. Matsugami, Solvation Structures of Tetraethylammonium Bromide and Tetrafluoroborate in Aqueous Binary Solvents with Ethanol, Trifluoroethanol, and Acetonitrile, J. Phys. Chem. B, 124 (2020) 5009-5020.

Supporting Information

Ionic conduction through single-pore and multipore polymer membranes in aprotic organic electrolytes

Saima Nasir[a,b], Mubarak Ali[a,b,*], Patricio Ramirez[c], Kristina Froehlich[a], Javier Cervera[d], Salvador Mafe[d], and Wolfgang Ensinger[a,e]

[a]*Department of Material- and Geo-Sciences, Materials Analysis, Technische Universität Darmstadt, Alarich-Weiss-Str. 02, D-64287 Darmstadt, Germany*

[b]*Materials Research Department, GSI Helmholtzzentrum für Schwerionenforschung, Planckstrasse 1, D-64291, Darmstadt, Germany*

[c]*Departament de Física Aplicada. Univ. Politècnica de València. E-46022 Valencia, Spain*

[d]*Departament de Física de la Terra i Termodinàmica, Universitat de València, E-46100 Burjassot, Spain*

[e]*Centre for Synthetic Biology, Technische Universität Darmstadt, 64283 Darmstadt, Germany*

*Corresponding authors:

Email address: m.ali@gsi.de

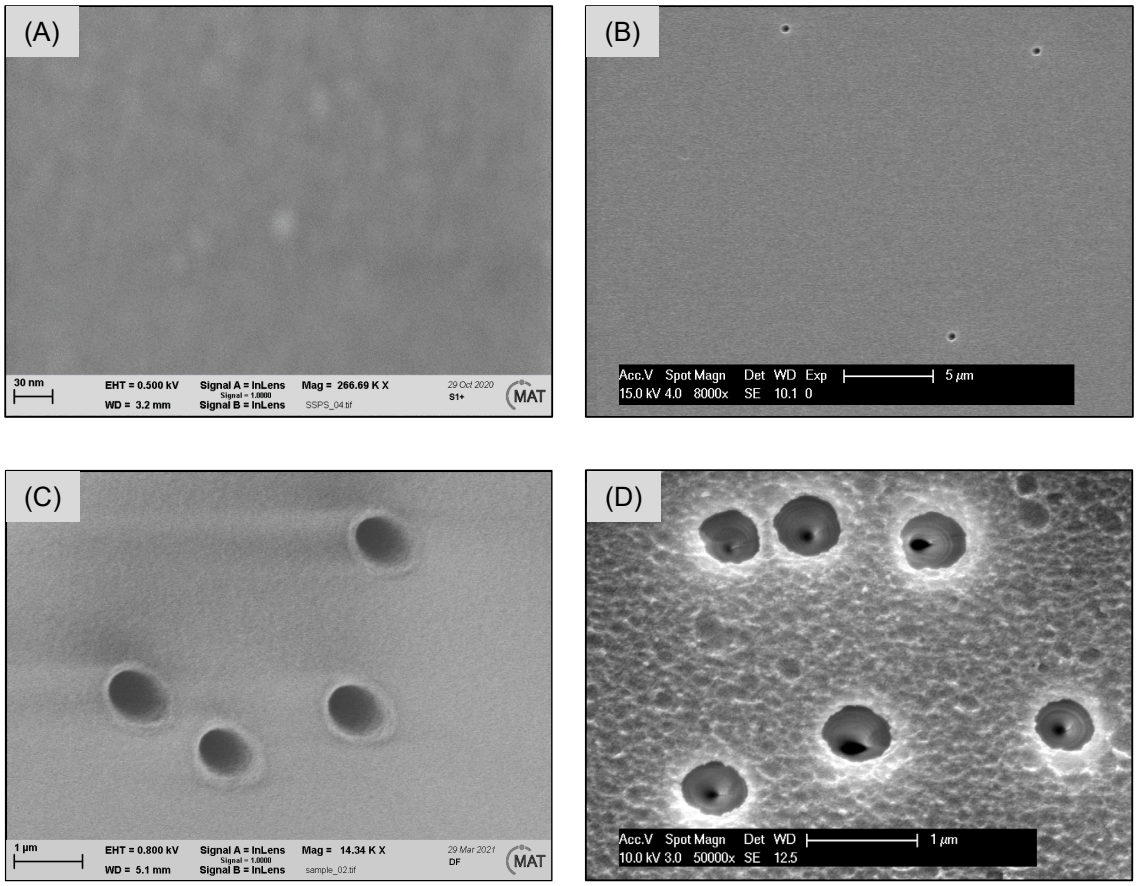

Figure S1. Scanning electron images of soft-etched (SE)-PI membrane having 10^9 ~~subnanometer~~ pores cm^{-2} (A), symmetric track-etched (TE)-PI membrane having 10^3 pores cm^{-2} (B), asymmetric track-etched PI membrane with 10^7 conical pores cm^{-2} (C) and asymmetric track-etched PET membrane with 10^7 conical pores cm^{-2} (D). Note that the pores in the SE-PI membrane (first image) are not visible under FESEM, which suggests a subnanometer size.

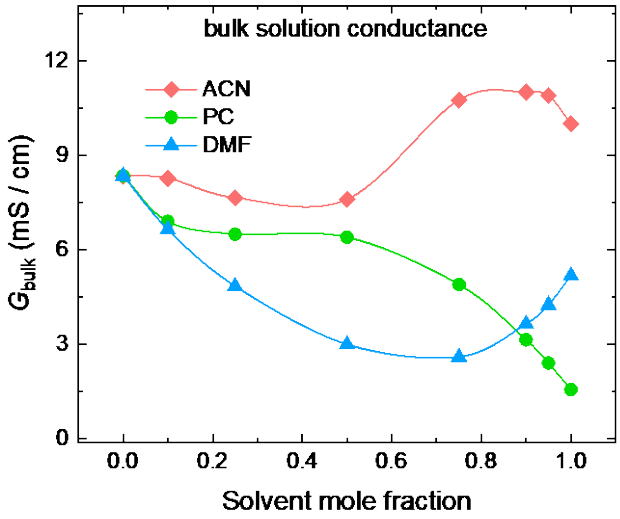

Figure S2. The bulk conductance of 0.1M $LiClO_4$ electrolyte solution as a function of the aprotic solvent mole fraction in water.

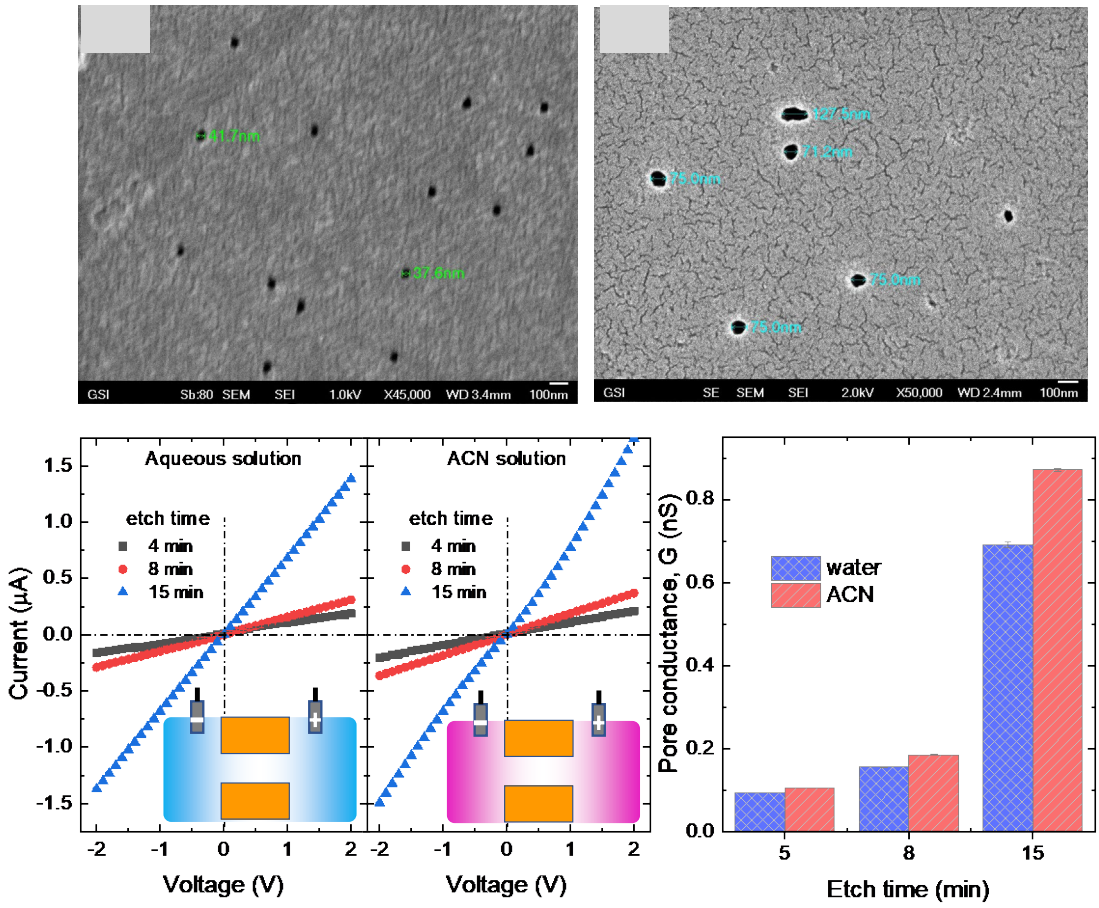

Figure S3. MUBARAK PLEASE CORRECT THIS CAPTION Scanning electron images of PET membrane having 10^8 pores cm^{-2} fabricated together with single pore-membrane for 8 min (A) and 15 min (B) under symmetrical track-etching conditions, Symmetric track-etched polyimide membrane having 10^3 pores cm^{-2} (B), asymmetric track-etched PI membrane with 10^7 conical pores cm^{-2} (C) and asymmetric track-etched PET membrane with 10^7 conical pores cm^{-2} (D). The *I–V* characteristics (C, D) and conductance (E) of single cylindrical nanopores in the PET membrane exposed to 0.1M $LiClO_4$ electrolyte solution prepared in water and anhydrous acetonitrile solvent.

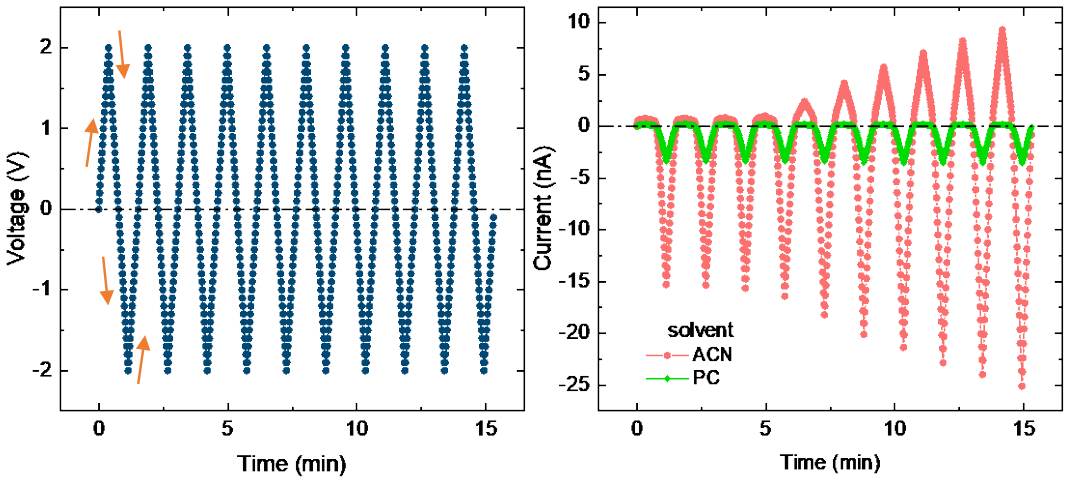

Figure S4. The voltage versus time input signal (A) and the resulting ionic current time trace (B) for the PI single conical nanopore in anhydrous acetonitrile and propylene carbonate solutions.

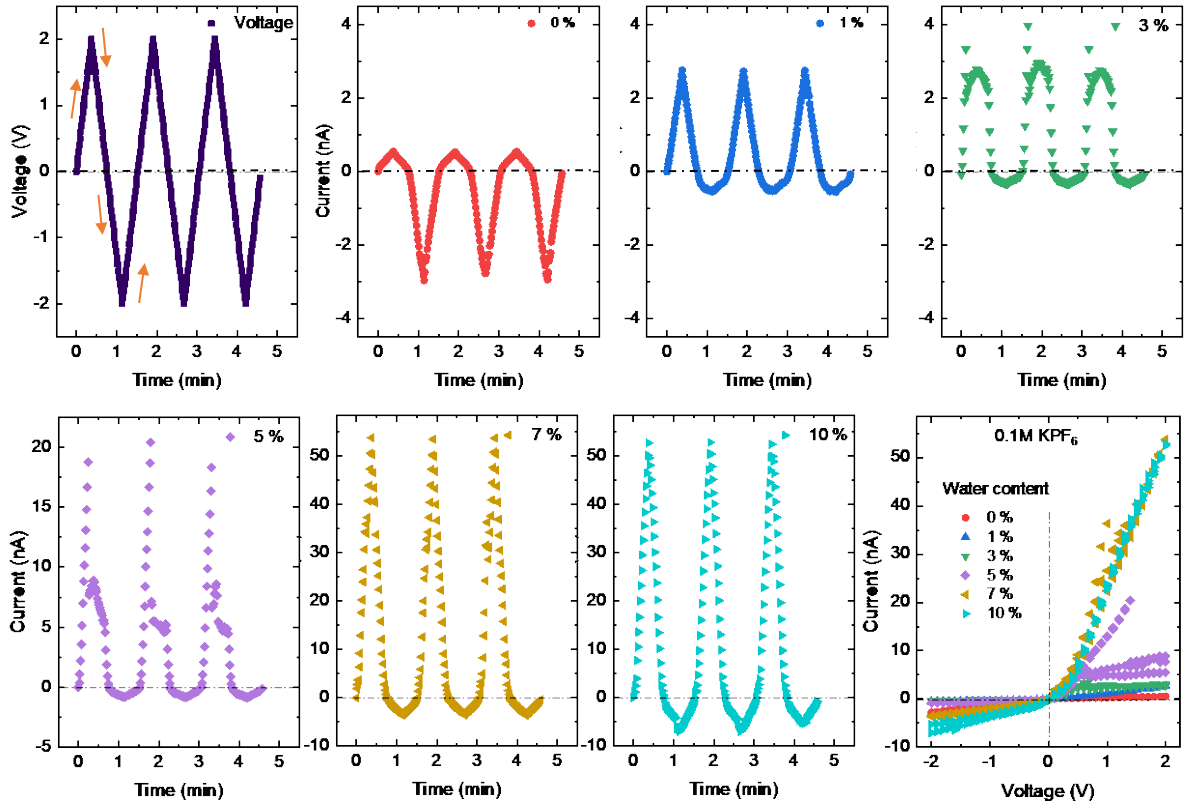

Figure S5. The voltage–time (A) and ion current–time (B –G) traces and the corresponding quasi-state *I–V* curves of the single conical nanopore in a 0.1M KPF_6 solution prepared in the PC solvent with the different water contents shown in the inset.

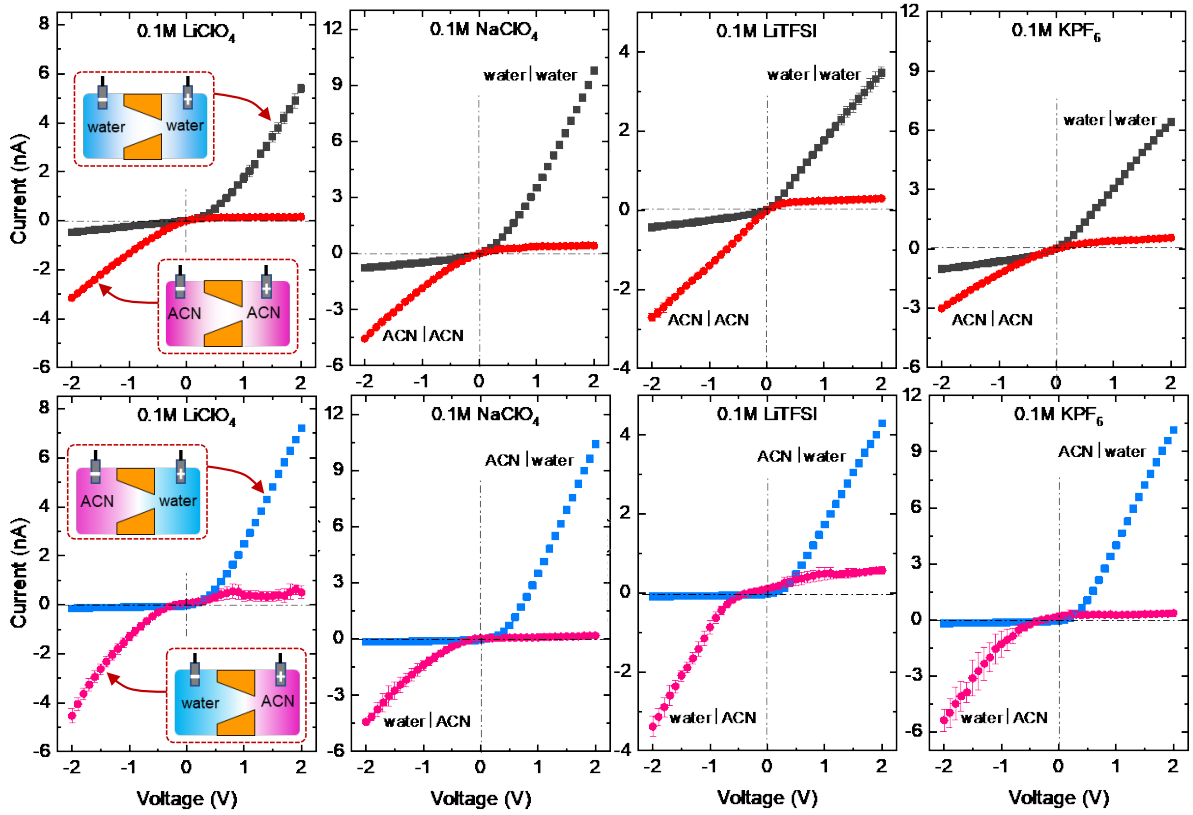

Figure S6. Changes in the *I–V* curves obtained with the PET single conical nanopore exposed to a 100 mM solution of different salts prepared in water and anhydrous acetonitrile under symmetric (A–D) and asymmetric electrolyte conditions (E–H).

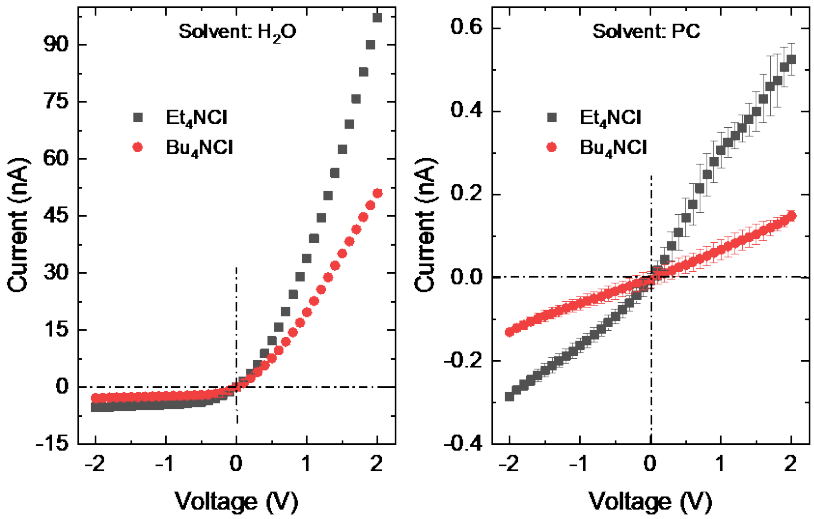

Figure S7. The *I–V* curves obtained with the PI single conical nanopore in 0.1M solution of alkylammonium chloride prepared in water (A) and anhydrous propylene carbonate (B).

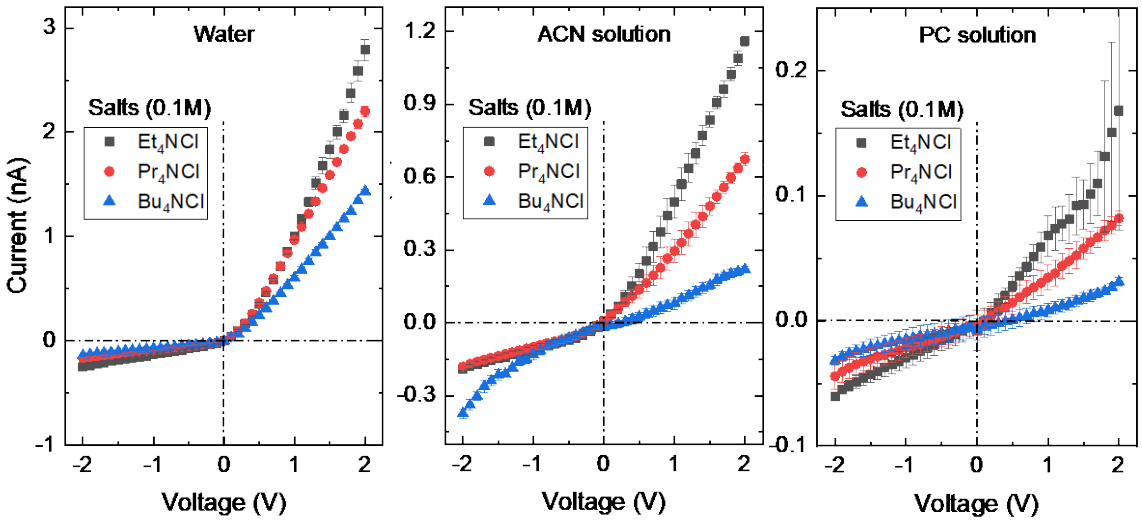

Figure S8. The *I–V* curves obtained with the PET single conical nanopore in 0.1M solution of different alkylammonium chloride salts prepared in water (A), anhydrous acetonitrile (B), and propylene carbonate (C).